Structure
Short Article

Preferential and Specific Binding of Human αB-Crystallin to a Cataract-Related Variant of γS-Crystallin

Carolyn N. Kingsley,[1,4] William D. Brubaker,[2,4] Stefan Markovic,[3] Anne Diehl,[3] Amanda J. Brindley,[1] Hartmut Oschkinat,[3] and Rachel W. Martin[1,2,*]
[1]Department of Chemistry, University of California, Irvine, Irvine, CA 92697-2025, USA
[2]Department of Molecular Biology and Biochemistry, University of California, Irvine, Irvine, CA 92697-3900, USA
[3]Leibniz-Institut Für Molekulare Pharmakologie, Berlin 13125, Germany
[4]These authors contributed equally to this work
*Correspondence: rwmartin@uci.edu
http://dx.doi.org/10.1016/j.str.2013.09.017

SUMMARY

Transparency in the eye lens is maintained via specific, functional interactions among the structural βγ- and chaperone α-crystallins. Here, we report the structure and α-crystallin binding interface of the G18V variant of human γS-crystallin (γS-G18V), which is linked to hereditary childhood-onset cortical cataract. Comparison of the solution nuclear magnetic resonance structures of wild-type and G18V γS-crystallin, both presented here, reveal that the increased aggregation propensity of γS-G18V results from neither global misfolding nor the solvent exposure of a hydrophobic residue but instead involves backbone rearrangement within the N-terminal domain. αB-crystallin binds more strongly to the variant, via a well-defined interaction surface observed via chemical shift differences. In the context of the αB-crystallin structure and the finding that it forms heterogeneous multimers, our structural studies suggest a potential mechanism for cataract formation via the depletion of the finite αB-crystallin population of the lens.

INTRODUCTION

The crystallins are the primary protein components of the eye lens, reaching concentrations higher than 400 mg/ml in humans (Tardieu et al., 1992). Short-range ordered interactions between crystallins at high concentrations are thought to maintain transparency while providing the refractive index gradient required to focus light on the retina (Delaye and Tardieu, 1983; Ponce et al., 2006). Perturbations to the intercrystallin interactions concomitant with the formation of high molecular weight aggregates can lead to lens opacification during aging and cataractogenesis. Characterizing the interactions between members of the two crystallin superfamilies, α- and βγ-crystallins, is critical to understanding cataract formation, because insoluble aggregates of crystallins from both have been found in cataractous lenses (Takemoto and Sorensen, 2008). The α-crystallins (αA and αB) act as holdase chaperones, binding to but not refolding structural βγ-crystallins for which solubility is compromised due to damage or mutation. Because of the extremely low protein turnover in lens fiber cells, the intercrystallin interactions are thus the first line of defense against aggregation. Mutations in either the α- or βγ crystallin genes can alter these critical attractive interactions (Fu and Liang, 2003). In the case of γC-crystallin, α-crystallins do not recognize all known disease-related variants (Moreau and King, 2012). Likewise, in γD-crystallin, both the E107A and R76S variants are implicated in early-onset cataract, but the former exhibits increased α-crystallin attraction (Banerjee et al., 2011), whereas α-crystallin interactions with the latter remain unchanged (Ji et al., 2012). Here, we focus on interactions between αB- and γS-crystallins: αB is the more versatile chaperone, abundantly expressed in tissues outside the eye lens (Iwaki et al., 1990), upregulated by various stressors (Klemenz et al., 1991), and implicated in several neuropathological diseases (Iwaki et al., 1989; van Noort et al., 1995; Ousman et al., 2007); whereas γS is the most abundant of the structural βγ-crystallins in the human lens cortex and is highly conserved across several species (Chang and Chang, 1987; Quax-Jeuken et al., 1985; van Rens et al., 1989, 1991).

At present, there are four known cataractogenic mutations in human γS-crystallin: the γS-V42M variant, which distorts the compact β sheet packing in the core of the N-terminal domain and causes severe congenital cataract in children (Vendra et al., 2012); the Coppock-cataract-associated γS-D26G variant, which leads to decreased protein stability but apparently has little effect on the overall molecular architecture (Karri et al., 2013); the γS-S39C variant, which is linked to microcornea and cataract (Devi et al., 2008) and which is hypothesized to have an exposed cysteine available for disulfide crosslinkage and aggregation; and the γS-G18V variant, which is implicated in childhood-onset cortical cataract (Sun et al., 2005). Although the decreased thermodynamic stability of γS-G18V relative to wild-type (γS-WT) (Ma et al., 2009) has been established, additional experiments indicated that it is aggregation prone well below its unfolding temperature, suggesting an aggregation mechanism more complex than simple denaturation (Brubaker et al., 2011). In order to better understand how structural changes in the cataract-related G18V variant of γS-crystallin lead to altered intermolecular interactions, we have solved the

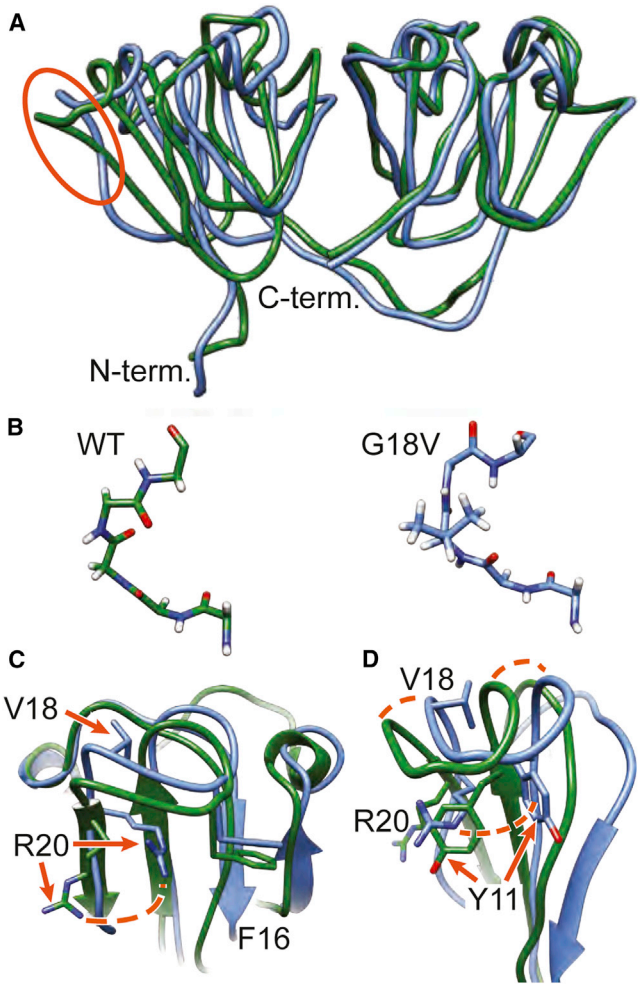

Figure 1. Structural Detail of Wild-Type and Variant γ-S Crystallin

(A and B) A licorice depiction of the average solution NMR structures of γS-WT (green) and γS-G18V (blue) is shown in (A). Both proteins are highly structured, with the double Greek key fold typical of structural crystallins, although the variant protein displays structural changes in the N-terminal (N-term.) domain (left) relative to wild-type (WT). The red circle indicates the region that is shown in greater detail in (B). Here, the affected loop remains essentially intact; in γS-WT (left) the α proton from G18 is angled slightly askew from the R19 amide proton. In γS-G18V, the orientation of the V18 methyls forces the amide proton into alignment with the valine side chain, altering the V18 Ψ angle. C-term., C-terminal.

(C) The overlaid structures of γS-WT (green) and γS-G18V (blue) with the side chains from F16, V18, and R20 shown, indicating the details of selected structural changes, particularly the dramatic shift in the position of R20.

(D) The addition of V18 and its effect on the backbone angles the former β strand outward and twists it, moving R20 inward, where it displaces Y11 and forces the tyrosine away from F16, placing it flat against the surface of the first Greek key motif. Although each of these structural changes is minor and has primarily local impact, taken in aggregate, they result in significant perturbations to the N-terminal domain, potentially providing sites for altered intermolecular interactions and recognition by αB-crystallin.

See also Figures S1–S4 and Tables S1 and S2.

solution nuclear magnetic resonance (NMR) structures of human wild-type and γS-G18V and elucidated the binding interface between αB-crystallin and γS-G18V.

Table 1. A Tabular Summary of the NMR Structures for γS-WT and γS- G18V Structures, Calculated Using Full Restraint Sets as Described in the Experimental Procedures

Restraint Summary and Structure Statistics	γS-WT	γS-G18V
Restraint Summary		
Total NOE restraints	7,444	4,682
Intraresidue	1,547	1,329
Interresidue		
Sequential ($\|i - j\| = 1$)	1,559	972
Medium range ($\|i - j\| \leq 5$)	1,286	709
Long range ($\|i - j\| \geq 6$)	3,052	1,672
Total angular restraints	408	450
RDCs	156	147
Dihedral (3J coupling)	–	57
Dihedral (TALOS+)	252	246
H-bond restraints	46	90
Structure Statistics (20 Lowest Energy Structures)		
Restraint violations		
NOE > 0.3 Å	0.6 ± 0.8	0.7 ± 1.1
Dihedral > 5°	1.1 ± 1.3	1.6 ± 0.9
RMSD from ideal covalent geometry		
Bonds (Å)	0.005 ± 0.000	0.004 ± 0.000
Angles (°)	0.582 ± 0.011	0.537 ± 0.016
Impropers (°)	0.503 ± 0.013	0.481 ± 0.016
Restraint RMSD		
NOE (Å)	0.034 ± 0.025	0.024 ± 0.002
Dihedral (°)	0.914 ± 0.137	0.893 ± 0.114
RDC (Hz)	0.238 ± 0.021	0.188 ± 0.018
Average pairwise RMSD (residues 5–178)		
Backbone RMSD (Å)	0.4	0.5
Heavy atom RMSD (Å)	0.8	0.9
RDC statistics		
R-factor (%)	0.642 ± 0.055	0.459 ± 0.046
R-factor (free) (%)	0.817 ± 0.073	0.556 ± 0.052

See also Figures S1–S4 and Tables S1 and S2.

RESULTS

The G18V Mutation Causes Structural Perturbation

Like the highly homologous murine protein (Wu et al., 2005) and other mammalian structural crystallins, γS-WT has a double Greek key fold. A comparison of the γS-WT and γS-G18V structures reveals local shifts in the backbone but little change in the overall fold. The average heavy-atom root-mean-square deviation (RMSD) between the two structures is 1.62 Å for the N-terminal domain and 1.13 Å for the C-terminal domain. (Figure 1; Table 1; Figures S1 and S2 and Tables S1 and S2 available online). Because G18 is located on a surface-exposed loop, solvent exposure of the valine side chain might be expected to provide a plausible mechanism for the solubility impact of this mutation; however, the structural data indicate that it is buried, with the backbone occupying an unusual conformation at this position. Many examples of residues stabilized by hydrogen bonds in

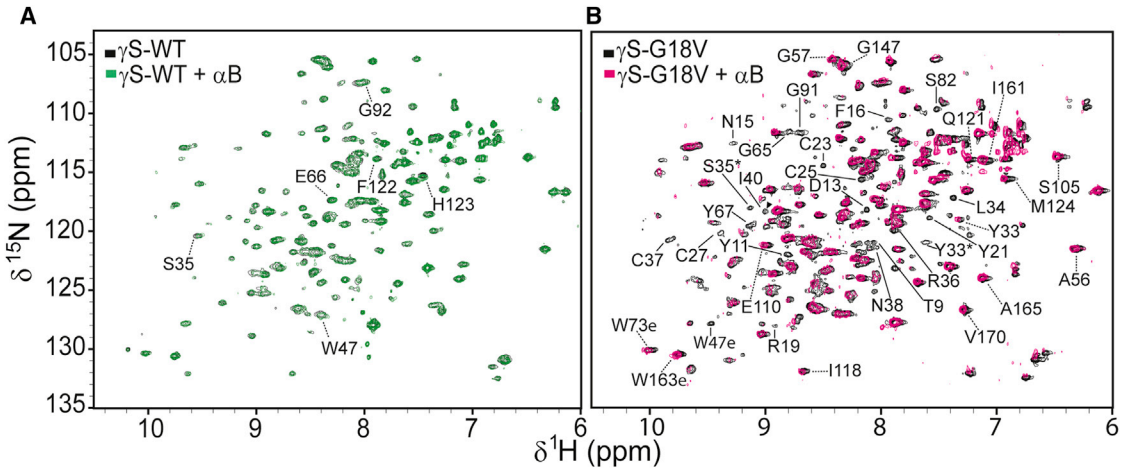

Figure 2. ^{15}N-^{1}H HSQCs of γS-WT and γS-G18V Bound to αB-Crystallin

(A and B) ^{15}N-^{1}H HSQCs of (A) ^{15}N-labeled γS-WT with (green) and without (black) αB and (B) ^{15}N-labeled γS-G18V with (pink) and without (black) αB. Dashed lines indicate cross-peaks that shift, whereas solid lines indicate cross-peaks that disappear with respect to the samples without αB. An asterisk indicates cross-peaks that belong to the alternate structure of γS-G18V. (Brubaker and Martin, 2012)

See also Table S1.

unfavorable Ramachandran angles (Jia et al., 1993; Gunasekaran et al., 1996) have been found in the context of enzyme active sites in which the conformation is required for activity (Jia et al., 1993; Pal and Chakrabarti, 2002). Here, the configuration of V18 is stabilized in part by the pi-stacking interactions between R20 and F16 (Figure 1C). The dihedral angles shift from $\phi = 79.3°$, $\psi = -146.4°$ for G18 to $\phi = 103.0°$, $\psi = -134.0°$ for V18. Presumably because of steric clashes with side chains on the opposing side of the affected loop, the methyls of V18 are angled toward the C-terminal end of the polypeptide chain, locking the R19 amide proton into place centered between the V18 methyls (Figure 1B). Additional structural calculations indicate that the V18 side chain remains buried even on exclusion of all distance restraints to V18, and the adoption of a favorable backbone dihedral angle configuration would require the elimination of restraints from several surrounding residues, producing an extensive structural disruption to the surrounding loop region that is not supported by the NMR data (Figure S3). The effect propagates down the polypeptide chain through more than half of the N-terminal domain of γS-crystallin. Despite these local differences, the overall folds of both structures are very similar (Figure 1A), consistent with previous circular dichroism and UV fluorescence data. Both γS-WT and γS-G18V were monomeric under the conditions used for structural NMR (Figure S4).

αB-Crystallin and γS-G18V Interact to Form Large Complexes

Because γS-G18V is implicated in early-onset cataract formation and has an altered structure in solution, we hypothesized that the molecular chaperone αB would interact more strongly with the disease-related variant than with wild-type γS. In order to assess the extent of binding, dynamic light scattering (DLS) measurements were performed at 25°C on samples of αB, γS-WT, and γS-G18V individually and as mixtures at pH 6.9. The DLS data are shown in Figure S5. These results are consistent with previous findings; human αB-crystallin spontaneously forms spherical multimers 80 to 180 Å in diameter with a variable number (~24–32) of subunits (Haley et al., 1998; Jehle et al., 2010). γS-WT has an average hydrodynamic diameter of 50.40 ± 0.28 Å, which is in agreement with reported values for other monomeric γ-crystallins (Liu et al., 1998). γS-G18V forms large multimers with diameters up to 289.2 ± 8.8 Å at pH 6.9. Mixtures of αB with γS-WT or γS-G18V have apparent hydrodynamic diameters up to 155.88 ± 0.46 and 478.2 ± 2.3 Å, respectively.

The size of the particles in the αB + γS-WT mixture is similar to that of αB alone, likely because there are only weak interactions between the two proteins, and the DLS size of the mixture thus reflects the much larger αB complexes. Conversely, the particle size of the αB + γS-G18V mixture is much larger than that of either γS-G18V or αB alone. This result indicates that αB is interacting more strongly with γS-G18V than with γS-WT and is consistent with the conclusions drawn by Abgar et al. (2001) that α-crystallin binds destabilized proteins to prevent nonspecific aggregation and that the resulting complex reorganizes into large particles in order to remain soluble.

αB-Crystallin Interacts More Strongly with γS-G18V

To localize the regions of γS-crystallin involved in interactions with αB, we performed heteronuclear single quantum coherence (HSQC) NMR spectroscopy on mixtures of ^{15}N-labeled γS-WT and γS-G18V with αB at pH 6.9. Solution NMR is sensitive to small changes in the electronic environment of the detected nuclei; therefore, binding interactions between αB and γS should result in shifts or disappearances of relevant cross-peaks. The addition of αB to ^{15}N-labeled γS-WT leads only to minor chemical shift changes in the ^{15}N-^{1}H HSQC spectrum recorded at 25°C (Figure 2A). Residues corresponding to cross-peaks that undergo minor chemical shift changes include S35, W47, E66, G92, F122, and H123—all surface residues. Furthermore, the lack of cross-peak disappearance in the presence of the molecular chaperone supports the conclusion that αB only weakly interacts with native γS in dilute solution, which is consistent

with the results of a past ^{1}H-NMR spectroscopic study of bovine α- and γS-crystallin (Cooper et al., 1994). In contrast, on addition of αB to ^{15}N-labeled γS-G18V, nearly 50% of the cross-peaks broadened below the noise threshold of the ^{15}N-^{1}H HSQC, presumably due to the formation of large αB/γS-G18V complexes in solution (expected to be >300 kDa). Using ^{15}N-^{1}H transverse-relaxation optimized spectroscopy (TROSY)-HSQC spectroscopy, we acquired a two-dimensional spectrum of the αB/γS-G18V mixture. Analysis of the resulting TROSY-HSQC of γS-G18V (Figure 2B) reveals the disappearance of several N-H cross-peaks; T9, Y11, D13, N15, F16, R19, Y21, C23, C25, C27, Y33*, L34, S35*, R36, C37, N38, I40, W47ε, G65, Y67, S82, S85, and G91. These residues are located in the N-terminal domain except for G91, which is situated in the linker between the two domains. It is interesting that the majority of cross-peaks that lose signal intensity correspond to γ-G18V residues that occupy different positions (and whose cross-peaks therefore shift) with respect to γS-WT. Y33* and S35* correspond to cross-peaks from a minor alternate conformation of γS-G18V, also previously assigned (Brubaker and Martin, 2012). There are several cross-peaks that slightly shift in the γS-G18V/αB mixture, including Y33, A56, G57, W73ε, S105, E110, I118, Q121, M124, G147, I161, W163ε, A165, and V170. These peaks are distributed throughout the protein and may shift due to altered surface interactions with αB and γS or due to changes in the local chemical environment resulting from the binding of αB and the associated formation of larger complexes.

Thermally Stressed γS-WT Does Not Recruit αB-Crystallin

Previous studies investigating the solubilizing capabilities of α-crystallin using γ-crystallin mixtures purified from bovine lenses have shown that α-crystallin can prevent the thermal aggregation of γ-crystallins (Horwitz, 1992). A similar study noted that the rate of protein aggregation was dependent on α-crystallin concentration and that, with a 3:2 α-:γ-crystallin ratio, using combinations of bovine α-crystallin and bovine γA-D, aggregation of the mixture occurred after heating at 72°C (Wang and Spector, 1995).

In light of these results and the finding that only weak binding was observed between human αB and γS-WT at 22°C, we set out to characterize the interactions between αB and γ-WT upon heating. An ^{15}N-^{1}H HSQC spectrum was taken every 5°C as γS-WT was heated between 22°C and 47°C, with and without αB. Sample precipitation and loss of signal occurred at temperatures above 47°C, consistent with our previous observation that wild-type γS-crystallin forms aggregates well below its unfolding temperature (Brubaker et al., 2011). In the spectra obtained for both γS-WT and the mixture of γS-WT + αB (shown overlaid in Figure 3), several cross-peaks of γS-WT shift due to temperature change. A direct comparison between the spectra of γS-WT in the presence and absence of αB (Figure 3A) reveals slight shifts and significant line broadening of the cross-peaks, which decrease with increasing temperature. However, no disappearance of cross-peaks is observed. The line broadening is due to weak transient interactions between αB and γS-WT, and its decrease with increasing temperature is attributed to accelerated molecular tumbling. Our observations of protein precipitation in the γS-WT/αB mixture at higher temperatures and the lack of disappearing cross-peaks in the HSQCs indicates that αB-crystallin does not recognize thermally unfolded γS-crystallin. Human αB crystallin retains its native secondary structure up to 70°C, although its chaperone activity is greatest near physiological temperatures (van Boekel et al., 1999; Reddy et al., 2000; Datta and Rao, 1999). This finding also suggests that thermal denaturation of native γS-crystallin is not a realistic model for cataract formation in this system.

DISCUSSION

Several three-dimensional (3D) structures of crystallins have been reported in the past decade, revealing the double Greek key fold as a common feature of βγ-crystallins (Jaenicke and Slingsby, 2001; Mills et al., 2007). The high stability and solubility of the crystallins is critical to their function because protein degradation and synthesis do not occur in mature differentiated lens fiber cells. Our results indicate that the relatively minor structural changes in γS-G18V result in a perturbation to the delicately balanced set of weak interactions between crystallins. The large body of structural investigations and interaction studies on β- and γ-crystallins suggests that specific interactions between them are functionally important (Slingsby et al., 1991). Weak interactions of individual βγ-clusters with α-crystallins may be relevant at the high protein concentrations in the eye lens, coupling these clusters to the structural dynamics of the polydisperse α-crystallin oligomers and preventing the formation of insoluble aggregates. Our observation of weak interactions between wild-type γS-crystallin and αB supports this hypothesis, because interactions should be weak, even at millimolar concentrations, to ensure an optimal level of exchange dynamics in the eye lens.

The spectra of the αB/γS-WT sample exhibited only minor chemical shift changes, and the affected residues are widely distributed throughout the structure (Figures 4A and 4B), confirming the presence of nonspecific interactions. In this context, we expect the protein interfaces to exhibit very weak binding at the relatively low concentrations investigated here. Conversely, αB interacts more strongly with the disease-related variant γS-G18V as evidenced by loss of cross-peak intensities and shifts due to the interactions with the chaperone. More quantitative comparison of the binding affinities presents experimental challenges, because binding to wild-type γS-crystallin is mainly characterized by line broadening rather than chemical shift differences. Furthermore, because αB-crystallin forms polydisperse oligomers alone and on binding to aggregation-prone substrates, its binding to wild-type and G18V γS-crystallin cannot be correctly described by a single dissociation constant. However, based on the NMR data, the interaction surface of γS-G18V that is recognized by αB-crystallin can be determined and is shown in Figures 4C and 4D. Residues of γS-G18V, whose cross-peaks lose intensity, are localized to the N-terminal domain, coincident with the greatest structural changes due to the V18 substitution. The additional weak interactions may play an important role in maintaining the solubility of the larger αB/γS-G18V complex.

In recognition of the results obtained with heat-denatured γS, as well as recent mass spectrometry analyses (Lampi et al., 2012), it appears that during the lifetime of the organism, the chaperone activity of α-crystallins is required to account for accumulated posttranslational modifications, such as

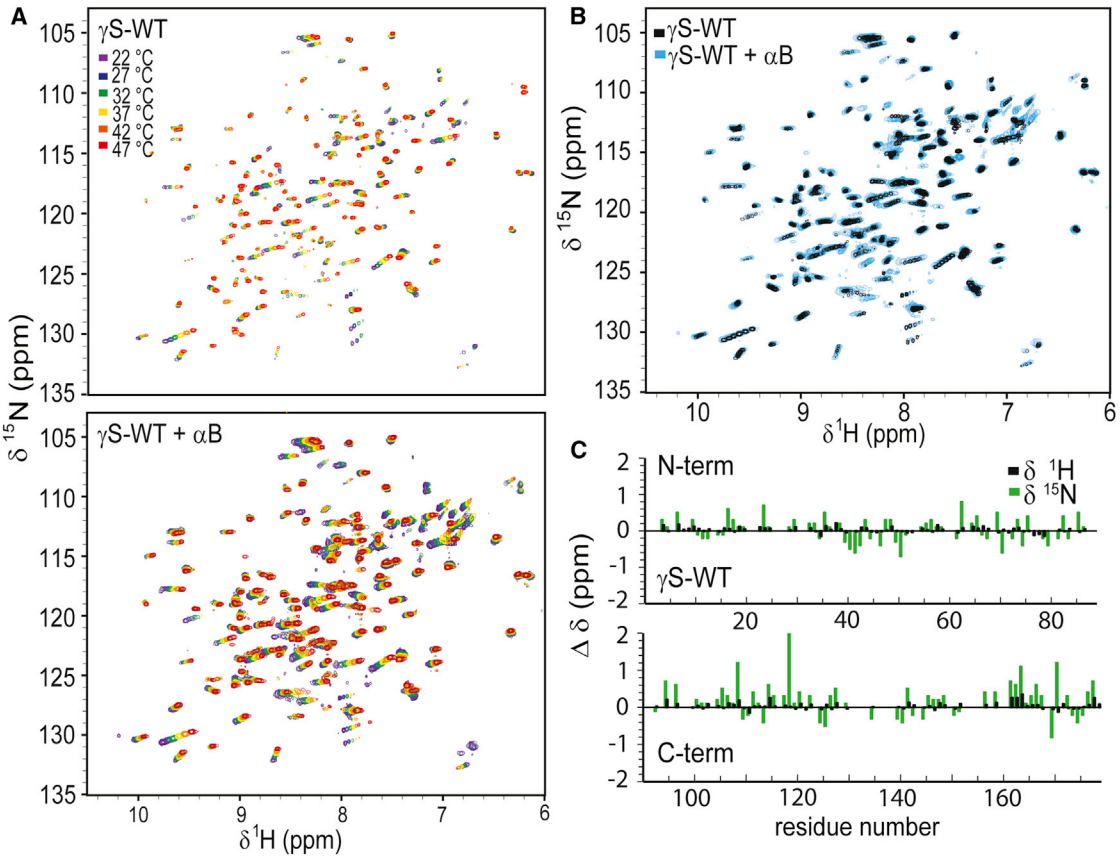

Figure 3. Solution NMR Data Indicating the Minor Conformational Changes in γS-WT on Heating and Its Weak, Nonspecific Interaction with αB-Crystallin

(A) ^{15}N-^{1}H HSQC temperature series from 22°C–47°C of γS-WT (top) and γS-WT + αB (bottom).

(B) Overlay of the γS-WT (black) and γS-WT + αB (blue) temperature series.

(C) Change in ^{15}N and ^{1}H resonances by residue of γS-WT between 22°C and 47°C.

deamidation or oxidation, rather than protein unfolding per se. Naturally occurring disease-related mutations represent a good model for this type of aggregation. Here, αB-crystallin interacts only weakly with γS-WT but more strongly and specifically with γS-G18V, as indicated by the differences in the NMR spectra between the two mixtures.

The stronger binding of αB to the variant is consistent with the hypothesis that the mechanism of cataractogenesis from the G18V mutation in γS-crystallin may be related to the depletion of the finite amount of α-crystallin in the eye lens. Given the deoptimization of binding strength in the γS-WT interactions, we speculate that many disease-related modifications or mutations cause the formation of tighter complexes with α-crystallins. In this way, α-crystallins perform a holdase chaperone function, preventing unfavorable interactions among β- and γ-crystallins. Additionally, disease onset may be accelerated due to both larger γS-G18V and αB–γS-G18V particles, which may be more prone to aggregation and precipitation. Similar effects were observed by others, reporting an increase in particle size after mixtures of α-crystallin and γ-crystallins from *D. mawsoni*, *T. obesus*, and *B. taurus* were heated extensively (Kiss et al., 2004). The exact mechanism that leads to this increase is yet unknown, but recruiting larger amounts of αB to the "sick" protein is likely, since an aggregation-prone or stability-relevant area requires additional protection by α-crystallin on top of any normal interactions. In this model, one role that α-crystallins may play in the eye lens is that of contributing a polydispersity principle preventing the formation of larger, more regular, and, ultimately, insoluble aggregates.

EXPERIMENTAL PROCEDURES

Sample Preparations

γS-WT, γS-G18V, and αB-crystallin were produced in *E. coli* and purified as described elsewhere (Brubaker et al., 2011; Brubaker and Martin, 2012; Jehle et al., 2010). NMR samples for structural work were at protein concentrations of 2.11 mM and 1.50 mM, respectively, in 10 mM acetate buffer, pH 4.5, 10% D_2O, 0.05% sodium azide, and 2 mM TMSP. Samples of γS-WT and γS-G18V under these conditions have remained stable and monomeric for over a year, showing no change in NMR spectra, when stored at 4°C. Samples for NMR studies with αB were at protein concentrations of 1.5 mM for both γS-WT and γS-G18V in 10 mM phosphate buffer, pH 6.9, 10% D_2O, 0.05% sodium azide. Mixed samples with αB-crystallin consisted of an αB:γS molar ratio of 2:1. All experiments except for ^{15}N in-phase, antiphase (IPAP) spectra and the spectra observing the αB/γS thermal interactions were collected at 22°C.

For residual dipolar coupling (RDC) measurements, the DIOTPC/DIOHPC bicelle system (Ottiger and Bax, 1999) at 10% (w/v) lipid concentration was used to align the protein samples. DIOTPC and DIOHPC disolved in chloroform

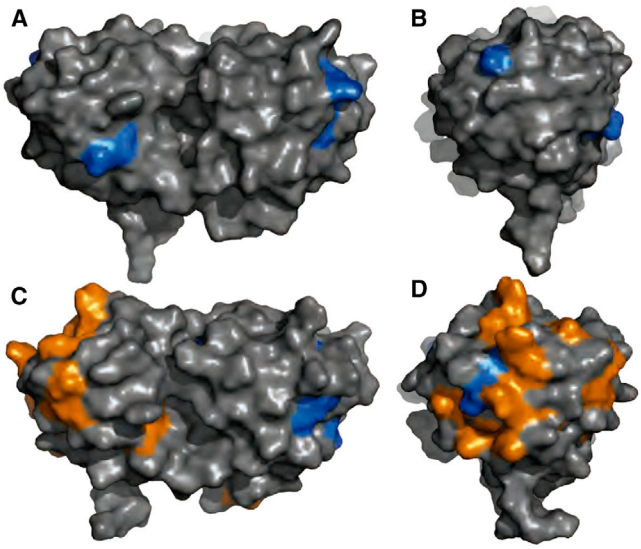

Figure 4. Residues of γS-WT Involved in Weak Transient Interactions with αB and γS-G18V Involved in Both Binding and Transient Interactions with αB

(A and B) Residues of γS-WT involved in weak transient interactions with αB are shown in blue on the surface of γS in two views: (a) view from the front and (b) with the N-terminal domain rotated forward.

(C and D) Residues of γS-G18V involved in binding interactions (orange) and transient interactions (blue) with αB shown on the surface of γS in two views: (C) from the front and (D) with the N-terminal domain rotated forward.

(Avanti Polar Lipids) were mixed at a molar ratio of 3:1 DIOTPC:DIOHPC and dried under a stream of nitrogen gas. The residual chloroform was removed by lyophilization. A 270 μl protein sample in 10 mM acetate buffer, pH 4.5, 10% D_2O, 0.05% sodium azide, and 2 mM TMSP was added to the lyophilized lipids. The sample was cycled several times between an ice bath and room temperature over the course of a few hours, with gentle mixing between each incubation to fully rehydrate the lipids and mix the bicelle sample.

Hydrogen-deuterium (H-D) exchange samples were prepared by concentrating the γS samples to saturation in centrifugal concentrator columns (with γS at a concentration of approximately 270 mg/ml at saturation) in a volume of approximately 60 μl and adding 99.9% D_2O to a total volume of 300 μl immediately before starting the data collection.

NMR Experiments

NMR experiments were performed on a Varian UnityINOVA system operating at 800 MHz equipped with a $^{1}H/^{13}C/^{15}N$ 5 mm tri-axis PFG triple-resonance probe. Decoupling of ^{15}N nuclei was performed by a GARP sequence (Shaka et al., 1985). ^{1}H shifts were referenced to TMSP, and ^{13}C and ^{15}N shifts were referenced indirectly to TMSP. Heated samples of αB/γS mixtures were equilibrated for several minutes before data acquisition. NMR data were processed using NMRPipe and analyzed using Sparky. H-D exchange spectra were taken at intervals of approximately 30 min for the first 4 hr following the addition of D_2O and then at intervals of 1 hr for the next 20 hr. Additional spectra were collected at intervals of several days. For each collection period, a one-dimensional proton spectrum was collected and nonexchanging methyls in the protein were used to adjust for differences in shimming between data collections.

Restraints

Nuclear Overhauser effect (NOE) restraints were assembled by manually picking slices from ^{13}C-filtered and ^{15}N-filtered NOE spectroscopy (NOESY) experiments corresponding to the ^{13}C and ^{15}N HSQC cross-peaks. The manually picked peaks were assigned in a binned fashion using three sets of chemical shift tolerances of decreasing stringency to minimize NOE cross-peak assignment ambiguity, and restraints were generated in CCPNMR Analysis. Duplicate and redundant restraints were eliminated from the exported restraint lists, and only unambiguous NOE restraints were used in the final structure calculations.

IPAP spectra of isotropic γS-WT and aligned γS-G18V were acquired at 32°C and 30°C. Each IPAP data set was processed into two spectra, each containing only one of the two doublet peaks so that all peaks could be easily resolved. For the RDCs, peaks were manually picked for all cross-peaks in the spectra, and the difference between the J splittings and the J+D splittings were computed for each resonance using a spreadsheet program. The starting error for all of the RDCs in the angular restraint table was set as the SD of the measured J splittings, 2.47 Hz and 3.01 Hz for γS-WT and γS-G18V, respectively. RDC experiments yielded 156 and 147 couplings for γS-WT and -G18V, respectively, including the side chain tryptophan Nε protons, corresponding to nearly every visible peak in the ^{1}H-^{15}N HSQC, which are included in the restraints deposited in the Protein Data Bank (PDB) (see Tables S1 and S2).

H-D exchange experiments yielded a total of 46 and 90 hydrogen bonding restraints used to refine the final structures for γS-WT and -G18V, respectively.

Dihedral angle restraints were calculated using the TALOS+ program (Shen et al., 2009) for γS-WT and for both the major and minor chemical shift sets of γS-G18V.

3J HN-HA couplings were calculated from peaks in a 3D H-N-HA experiment and were used as restraints in structure calculations for the γS-WT and γS-G18V structures (Table 1).

ACCESSION NUMBERS

The solution NMR structures of γS-WT and γS-G18V have been deposited in the PDB with IDs 2M3T and 2M3U, respectively.

SUPPLEMENTAL INFORMATION

Supplemental Information includes Supplemental Experimental Procedures, five figures, two tables, and two 3D molecular model files and can be found with this article online at http://dx.doi.org/10.1016/j.str.2013.09.017.

AUTHOR CONTRIBUTIONS

C.N.K. and W.D.B. prepared protein samples, performed NMR and DLS experiments, analyzed NMR and DLS data, and wrote the manuscript; S.M., A.D., and A.J.B. prepared protein samples; and H.O. and R.W.M. designed the experiments, analyzed data, and wrote the manuscript.

ACKNOWLEDGMENTS

We thank Wytze van der Veer for assistance with optical data collection and Doug Tobias and Melanie Cocco for helpful discussions. This work was supported by National Institutes of Health grant 1R01EY021514 (to R.W.M.) and a Deutsche Forschungsgemeinschaft grant within the frame of the SFB 740 (to H.O.).

Received: August 5, 2013
Revised: September 19, 2013
Accepted: September 23, 2013
Published: October 31, 2013

REFERENCES

Abgar, S., Vanhoudt, J., Aerts, T., and Clauwaert, J. (2001). Study of the chaperoning mechanism of bovine lens alpha-crystallin, a member of the alpha-small heat shock superfamily. Biophys. J. *80*, 1986–1995.

Banerjee, P.R., Pande, A., Patrosz, J., Thurston, G.M., and Pande, J. (2011). Cataract-associated mutant E107A of human gammaD-crystallin shows increased attraction to α-crystallin and enhanced light scattering. Proc. Natl. Acad. Sci. USA *108*, 574–579.

Brubaker, W.D., and Martin, R.W. (2012). ^{1}H, ^{13}C, and ^{15}N assignments of wild-type human γS-crystallin and its cataract-related variant γS-G18V. Biomol. NMR Assign. *6*, 63–67.

Brubaker, W.D., Freites, J.A., Golchert, K.J., Shapiro, R.A., Morikis, V., Tobias, D.J., and Martin, R.W. (2011). Separating instability from aggregation propensity in γS-crystallin variants. Biophys. J. *100*, 498–506.

Chang, T., and Chang, W.C. (1987). Cloning and sequencing of a carp beta s-crystallin cDNA. Biochim. Biophys. Acta *910*, 89–92.

Cooper, P.G., Carver, J.A., Aquilina, J.A., Ralston, G.B., and Truscott, R.J. (1994). A ^{1}H NMR spectroscopic comparison of γ S- and γ B-crystallins. Exp. Eye Res. *59*, 211–220.

Datta, S.A., and Rao, C.M. (1999). Differential temperature-dependent chaperone-like activity of alphaA- and alphaB-crystallin homoaggregates. J. Biol. Chem. *274*, 34773–34778.

Delaye, M., and Tardieu, A. (1983). Short-range order of crystallin proteins accounts for eye lens transparency. Nature *302*, 415–417.

Devi, R.R., Yao, W., Vijayalakshmi, P., Sergeev, Y.V., Sundaresan, P., and Hejtmancik, J.F. (2008). Crystallin gene mutations in Indian families with inherited pediatric cataract. Mol. Vis. *14*, 1157–1170.

Fu, L., and Liang, J.J.-N. (2003). Alteration of protein-protein interactions of congenital cataract crystallin mutants. Invest. Ophthalmol. Vis. Sci. *44*, 1155–1159.

Gunasekaran, K., Ramakrishnan, C., and Balaram, P. (1996). Disallowed Ramachandran conformations of amino acid residues in protein structures. J. Mol. Biol. *264*, 191–198.

Haley, D.A., Horwitz, J., and Stewart, P.L. (1998). The small heat-shock protein, alphaB-crystallin, has a variable quaternary structure. J. Mol. Biol. *277*, 27–35.

Horwitz, J. (1992). Alpha-crystallin can function as a molecular chaperone. Proc. Natl. Acad. Sci. USA *89*, 10449–10453.

Iwaki, T., Kume-Iwaki, A., Liem, R.K., and Goldman, J.E. (1989). Alpha B-crystallin is expressed in non-lenticular tissues and accumulates in Alexander's disease brain. Cell *57*, 71–78.

Iwaki, T., Kume-Iwaki, A., and Goldman, J.E. (1990). Cellular distribution of alpha B-crystallin in non-lenticular tissues. J. Histochem. Cytochem. *38*, 31–39.

Jaenicke, R., and Slingsby, C. (2001). Lens crystallins and their microbial homologs: structure, stability, and function. Crit. Rev. Biochem. Mol. Biol. *36*, 435–499.

Jehle, S., Rajagopal, P., Bardiaux, B., Markovic, S., Kühne, R., Stout, J.R., Higman, V.A., Klevit, R.E., van Rossum, B.J., and Oschkinat, H. (2010). Solid-state NMR and SAXS studies provide a structural basis for the activation of alphaB-crystallin oligomers. Nat. Struct. Mol. Biol. *17*, 1037–1042.

Ji, F., Jung, J., and Gronenborn, A.M. (2012). Structural and biochemical characterization of the childhood cataract-associated R76S mutant of human γD-crystallin. Biochemistry *51*, 2588–2596.

Jia, Z., Vandonselaar, M., Quail, J.W., and Delbaere, L.T. (1993). Active-centre torsion-angle strain revealed in 1.6 A-resolution structure of histidine-containing phosphocarrier protein. Nature *361*, 94–97.

Karri, S., Kasetti, R.B., Vendra, V.P.R., Chandani, S., and Balasubramanian, D. (2013). Structural analysis of the mutant protein D26G of human γS-crystallin, associated with Coppock cataract. Mol. Vis. *19*, 1231–1237.

Kiss, A.J., Mirarefi, A.Y., Ramakrishnan, S., Zukoski, C.F., Devries, A.L., and Cheng, C.-H.C. (2004). Cold-stable eye lens crystallins of the Antarctic notothenioid toothfish Dissostichus mawsoni Norman. J. Exp. Biol. *207*, 4633–4649.

Klemenz, R., Fröhli, E., Steiger, R.H., Schäfer, R., and Aoyama, A. (1991). Alpha B-crystallin is a small heat shock protein. Proc. Natl. Acad. Sci. USA *88*, 3652–3656.

Lampi, K.J., Fox, C.B., and David, L.L. (2012). Changes in solvent accessibility of wild-type and deamidated βB2-crystallin following complex formation with αA-crystallin. Exp. Eye Res. *104*, 48–58.

Liu, C., Pande, J., Lomakin, A., Ogun, O., and Benedek, G.B. (1998). Aggregation in aqueous solutions of lens γ-crystallins: special role of γS- crystallin. Invest. Ophthalmol. Vis. Sci. *39*, 1609–1619.

Ma, Z., Piszczek, G., Wingfield, P.T., Sergeev, Y.V., and Hejtmancik, J.F. (2009). The G18V CRYGS mutation associated with human cataracts increases gammaS-crystallin sensitivity to thermal and chemical stress. Biochemistry *48*, 7334–7341.

Mills, I.A., Flaugh, S.L., Kosinski-Collins, M.S., and King, J.A. (2007). Folding and stability of the isolated Greek key domains of the long-lived human lens proteins gammaD-crystallin and gammaS-crystallin. Protein Sci. *16*, 2427–2444.

Moreau, K.L., and King, J.A. (2012). Cataract-causing defect of a mutant γ-crystallin proceeds through an aggregation pathway which bypasses recognition by the α-crystallin chaperone. PLoS ONE *7*, e37256.

Ottiger, M., and Bax, A. (1999). Bicelle-based liquid crystals for NMR-measurement of dipolar couplings at acidic and basic pH values. J. Biomol. NMR *13*, 187–191.

Ousman, S.S., Tomooka, B.H., van Noort, J.M., Wawrousek, E.F., O'Connor, K.C., Hafler, D.A., Sobel, R.A., Robinson, W.H., and Steinman, L. (2007). Protective and therapeutic role for alphaB-crystallin in autoimmune demyelination. Nature *448*, 474–479.

Pal, D., and Chakrabarti, P. (2002). On residues in the disallowed region of the Ramachandran map. Biopolymers *63*, 195–206.

Ponce, A., Sorensen, C., and Takemoto, L. (2006). Role of short-range protein interactions in lens opacifications. Mol. Vis. *12*, 879–884.

Quax-Jeuken, Y., Driessen, H., Leunissen, J., Quax, W., de Jong, W., and Bloemendal, H. (1985). beta s-Crystallin: structure and evolution of a distinct member of the beta gamma-superfamily. EMBO J. *4*, 2597–2602.

Reddy, G.B., Das, K.P., Petrash, J.M., and Surewicz, W.K. (2000). Temperature-dependent chaperone activity and structural properties of human alphaA- and alphaB-crystallins. J. Biol. Chem. *275*, 4565–4570.

Shaka, A.J., Barker, P.B., and Freeman, R. (1985). Computer optimized decoupling scheme for wideband applications and low-level operation. J. Magn. Reson. *64*, 547–552.

Shen, Y., Delaglio, F., Cornilescu, G., and Bax, A. (2009). TALOS+: a hybrid method for predicting protein backbone torsion angles from NMR chemical shifts. J. Biomol. NMR *44*, 213–223.

Slingsby, C., Simpson, A., Ferszt, A., Bateman, O.A., and Nalini, V. (1991). Molecular interactions in the eye lens. Biochem. Soc. Trans. *19*, 853–858.

Sun, H., Ma, Z., Li, Y., Liu, B., Li, Z., Ding, X., Gao, Y., Ma, W., Tang, X., Li, X., and Shen, Y. (2005). Gamma-S crystallin gene (CRYGS) mutation causes dominant progressive cortical cataract in humans. J. Med. Genet. *42*, 706–710.

Takemoto, L., and Sorensen, C.M. (2008). Protein-protein interactions and lens transparency. Exp. Eye Res. *87*, 496–501.

Tardieu, A., Vérétout, F., Krop, B., and Slingsby, C. (1992). Protein interactions in the calf eye lens: interactions between beta-crystallins are repulsive whereas in gamma-crystallins they are attractive. Eur. Biophys. J. *21*, 1–12.

van Boekel, M.A., de Lange, F., de Grip, W.J., and de Jong, W.W. (1999). Eye lens alphaA- and alphaB-crystallin: complex stability versus chaperone-like activity. Biochim. Biophys. Acta *1434*, 114–123.

van Noort, J.M., van Sechel, A.C., Bajramovic, J.J., el Ouagmiri, M., Polman, C.H., Lassmann, H., and Ravid, R. (1995). The small heat-shock protein α B-crystallin as candidate autoantigen in multiple sclerosis. Nature *375*, 798–801.

van Rens, G.L., Raats, J.M., Driessen, H.P., Oldenburg, M., Wijnen, J.T., Khan, P.M., de Jong, W.W., and Bloemendal, H. (1989). Structure of the bovine eye lens gamma s-crystallin gene (formerly beta s). Gene *78*, 225–233.

van Rens, G.L., De Jong, W.W., and Bloemendal, H. (1991). One member of the gamma-crystallin gene family, gamma s, is expressed in birds. Exp. Eye Res. *53*, 135–138.

Vendra, V.P., Chandani, S., and Balasubramanian, D. (2012). The mutation V42M distorts the compact packing of the human gamma-S-crystallin molecule, resulting in congenital cataract. PLoS ONE *7*, e51401.

Wang, K., and Spector, A. (1995). α-crystallin can act as a chaperone under conditions of oxidative stress. Invest. Ophthalmol. Vis. Sci. *36*, 311–321.

Wu, Z., Delaglio, F., Wyatt, K., Wistow, G., and Bax, A. (2005). Solution structure of (gamma)S-crystallin by molecular fragment replacement NMR. Protein Sci. *14*, 3101–3114.